Synthesis of magnetic Fe_3O_4 particles covered with a modifiable phospholipid coat

2003 J. Phys.: Condens. Matter 15 S1425

(http://iopscience.iop.org/0953-8984/15/15/308)

INSTITUTE OF PHYSICS PUBLISHING JOURNAL OF PHYSICS: CONDENSED MATTER

J. Phys.: Condens. Matter **15** (2003) S1425–S1436 PII: S0953-8984(03)52757-6

Synthesis of magnetic Fe_3O_4 particles covered with a modifiable phospholipid coat

M De Cuyper[1], P Müller[2], H Lueken[2] and M Hodenius[2]

[1] Interdisciplinary Research Centre, Katholieke Universiteit Leuven-Campus Kortrijk, B-8500 Kortrijk, Belgium
[2] Rheinisch-Westfälische Technische Hochschule Aachen, Prof.-Pirlet-Straße 1, D-52074 Aachen, Germany

Received 27 August 2002
Published 7 April 2003
Online at stacks.iop.org/JPhysCM/15/S1425

Abstract

This work reports the synthesis of iron oxide cores by coprecipitation of Fe^{2+} and Fe^{3+} ions with $NaHCO_3$ or NH_3. Depending on the experimental conditions, particles of two different sizes (13 or 130 nm diameter) were produced. X-ray diffractometry revealed Fe_3O_4 (magnetite) to be the main constituent. The smaller particles, which, in contrast to the larger ones, are superparamagnetic, were stabilized with a phospholipid bilayer consisting of a 9:1 molar ratio of dimyristoylphosphatidylcholine and dimyristoylphosphatidylglycerol, thereby creating so-called magnetoliposomes. In a subsequent step, poly(ethylene glycol)-(PEG-) derivatized dipalmitoylphosphatidylethanolamine was introduced into the lipid envelope by incubating the magnetoliposomes with preformed sonicated vesicles containing the PEGylated lipid. The mechanism by which lipid transfer occurred was determined from the kinetic profiles. The relevance of these observations to a wide range of biomedical applications is briefly discussed.

1. Introduction

Liposomes are biocolloidal structures that consist of one or more spherical phospholipid bilayers suspended in an aqueous environment and with diameters ranging from 30 to about 1000 nm. Since their development in the mid-1960s by Bangham *et al* [1], the range of liposome types has considerably expanded and it is now possible to engineer liposomes of a size, phospholipid composition and surface characteristics to suit any specific application. In this context, in the late 1980s, we developed so-called 'magnetoliposomes', i.e. small unilamellar vesicles (SUVs) of which the aqueous interior is completely occupied by a magnetizable iron oxide grain [2]. The approach to generate these structures was rather new. Indeed, instead of incorporating magnetic substances into the inner aqueous space of the vesicles during their preparation (as used, for example, for the encapsulation of water-soluble drugs—[3]), we started with a surfactant-coated magnetic core on to which we adsorbed a phospholipid bilayer.

We subsequently showed that these structures could be successfully used in magnetically controlled bioreactors [4] and for selected *in vivo* applications, e.g. as contrast agents in magnetic resonance imaging [5]. In addition, Müller-Schulte *et al* [6] proposed the use of these structures for local hyperthermia therapy, after intravenous injection of the particles and subsequently putting the malignant tissue in an alternating magnetic field.

However, the further exploitation of these structures in selected fields of modern biotechnology and in diagnostic and therapeutic biomedicine requires the fundamental characterization of both the iron oxide core and the lipid envelope. Both have been studied in the present work. Firstly, using the co-precipitation technique, we synthesized two types of iron oxide grain with different sizes and compared their crystal structures, magnetization profiles and magnetic remanence. Secondly, after coating the particles with a phospholipid bilayer, we monitored the exchangeability of individual phospholipid molecules between vesicle donors and magnetoliposome acceptors. In this way, it should be feasible to carefully tune the surface properties of the magnetic biocolloids. In this context, it is well known that the phospholipid nature of the coat guaranties a high biocompatibility, making magnetoliposomes unique candidates for *in vivo* use. Unfortunately, however, after intravenous injection, classical vesicles (as well as magnetoliposomes) are removed relatively quickly from the bloodstream by liver cells [5, 7]. To circumvent this undesired event, Allen [7] incorporated a small percentage of poly(ethylene glycol)-(PEG-) derivatized phospholipids into the liposome membrane. The present work describes how these PEGylated phospholipids can be incorporated in an elegant way into the lipid coat surrounding the iron oxide core.

2. Experimental details

2.1. Materials

$FeCl_2{\cdot}4H_2O$ and $FeCl_3{\cdot}6H_2O$ were obtained from Merck (Darmstadt, Germany), Tiron (4, 5-dihydroxy-1, 3-benzenedisulfonic acid, disodium salt) from Acros Organics (Geel, Belgium) and 2-*T*(hydroxymethyl)methyl-aminoethanesulfonic acid (TES) from Sigma (St Louis, MO, USA). α-biotinylamido-ω-N-succinimidoxycarbonyl-poly(ethylene glycol), with a weight average of approximately 3400 Da (NHS-PEG_{3400}-B), was from Shearwater Polymers (Huntsville, AL, USA). Dimyristoylphosphatidylcholine (DMPC), dimyristoylphosphatidyl-glycerol (DMPG) and dipalmitoylphosphatidylethanolamine (DPPE) were from Avanti Polar Lipids Inc. (Birmingham, AL, USA). DPPE-PEG_{3400}-B was synthesized as described previously [8]. All other chemicals were from Merck (*pro analysi* quality).

2.2. Methods

2.2.1. Preparation of iron oxide cores. The iron oxide cores were prepared as described by Khalafalla and Reimers (method KR) [9] and Bergemann (method B) [10]. In method KR, 16.7 ml of a 25% NH_3 solution was added dropwise at room temperature to a freshly prepared solution of 8 g (30 mmol) of $FeCl_3{\cdot}6H_2O$ and 4 g (20 mmol) of $FeCl_2{\cdot}4H_2O$ in 33 ml of deionized water (Fe^{3+}/Fe^{2+} molar ratio 3/2), while stirring the mixture rapidly with a mechanical paddle [9]. Iron oxide formed immediately as a black magnetic precipitate. After 2 min, the supernatant was decanted by inversion of the reaction vessel placed on a permanent magnet, then 50 ml of 10^{-4} mol l^{-1} NH_4OH was added to the precipitate. After stirring for 2 min, the iron oxide was separated from the clear supernatant by magnetic decantation. This procedure was repeated six times, resulting in the removal of chloride ions from the supernatant, as checked by addition of 65% HNO_3 and a drop of 30% $AgNO_3$.

In method B, 1.8 g (6.8 mmol) of $FeCl_3 \cdot 6H_2O$ and 0.9 g (4.5 mmol) of $FeCl_2 \cdot 4H_2O$ were dissolved at 70 °C in 9 ml of deionized water, then, while maintaining this temperature, the pH was increased to 7.0 by slow addition of a solution of 4.1 g (49 mmol) of $NaHCO_3$ in 44.6 ml of deionized water. The reaction mixture was then quickly heated to boiling temperature, resulting in the formation of iron oxide as a black precipitate within 30 min. After cooling to room temperature, the precipitate was washed with 10^{-4} mol l^{-1} NaOH using the decantation method described above (method KR).

2.2.2. Characterization of the iron oxide cores. To completely remove water from the samples to be used for x-ray diffractometry and magnetization measurements, the iron oxide cores were pre-dried in a high vacuum (10^{-6} mbar), then heated at 80 °C for 2 h.

The x-ray patterns were taken on a Huber image-plate diffractometer (G 670, Huber, Darmstadt, Germany). The powders were exposed for 90 min at room temperature to Cu $K\alpha_1$ radiation ($\lambda = 154.056$ pm) as flat samples in air. The reflections were indexed by comparison with the theoretical 2θ values, calculated using the program Lazy Pulverix [11] on the basis of literature data for the cubic structures of Fe_3O_4 [12] and γ-Fe_2O_3 [13]. The mean diameter ($\overline{\varnothing}$) of the crystallites was determined from the reflection broadening, using Scherrer's formula [14]

$$\overline{\varnothing} = \frac{0.9\lambda}{\beta \cos\theta} \tag{1}$$

where β represents the reflection half-width caused by the crystal size. In practice, apparatus-dependent influences lead to additional reflection broadening and correction of the experimental values is required [15]. To do so, a polycrystalline standard sample was subjected to the process described above. The standard sample was prepared by annealing some of the iron oxide cores prepared by method B at 870 °C for 24 h in a high vacuum.

The magnetic moments were measured at room temperature on a SQUID magnetometer (MPMS-5S, Quantum Design, San Diego, CA, USA) using $HgCo(NCS)_4$ as standard [16]. To determine the magnetization (σ) and hysteresis, the applied field (B_0) was first gradually increased from 0 to +2 T, then shifted from +2 to −2 T, and finally from −2 to 0 T. The powder sample (5.9 mg for the KR preparation; 2.6 mg for the B preparation) was pressed into a quartz tube by a piston to prevent the sample moving in the capsule.

2.2.3. Preparation of phospholipid vesicles. The chloroform, used as a solvent for the various phospholipid types, was evaporated in a stream of nitrogen, the lipid film left overnight under vacuum to remove traces of organic solvent and the resulting dried lipids dispersed in TES buffer (5 mM, pH 7.0). To obtain SUVs, the lipid/buffer mixture was sonicated with a titanium probe-tip sonicator (MSE, 150 W) for 10 min (25 °C) at a power setting at which no frothing and only minimal disturbance of the solution surface occurred. After sonication, the vesicles were centrifuged for 10 min to remove residual titanium particles (Sorvall RC-5B, SS-34 rotor, 5000 rpm).

2.2.4. Preparation of magnetoliposomes. Particles prepared by the KR method were stabilized, both sterically and electrostatically, by adding 1.5 g of solid lauric acid while maintaining the temperature at 90 °C to improve the solubility of the detergent [9]. Then, the lauric acid was substituted by phospholipids using dialysis (membrane molecular weight cut-off 12 000 Da) of Fe_3O_4–lauric acid complexes (47 mg of Fe_3O_4) for three days at 37 °C in the presence of vesicles (228 mg of phospholipid), prepared as described above. After dialysis, non-adsorbed phospholipids were removed by high-gradient magnetophoresis (Bruker BE15 electromagnet, Karlsruhe, Germany) as described previously [2].

2.2.5. Phospholipid transfer. Mixtures for kinetic studies were prepared by incubating equal volumes of magnetoliposomes and SUVs, both at a phospholipid concentration of 0.8 μmol ml^{-1}. Separation of both types of nanocolloid was done at regular times by high-gradient magnetophoresis [2]. The eluate (vesicles) and retentate (magnetoliposomes) fractions of each sample were analysed for iron and phospholipid content and fatty acid composition. The data points were analysed by the first-order reaction formalism (see appendix). The first-order rate constant for lipid transfer, k_{+1}, was calculated from the following formula:

$$\ln \Delta x = \ln(\Delta x)_0 - 2k_{+1}t \tag{2}$$

where Δx and $(\Delta x)_0$ denote the deviation from equilibrium of the PEGylated lipid fraction in the outer shell of the phospholipid bilayer at $t = t$ and 0, respectively.

2.2.6. Assays. Determination of the iron content was carried out by dissolving the dried iron oxide cores in 37% hydrochloric acid/65% nitric acid (v/v 3/1), then quantifying Fe^{3+} colorimetrically at 480 nm after chelation with Tiron [17]. The phospholipid content of vesicle and magnetoliposome suspensions was quantified colorimetrically (820 nm) by phosphate analysis, using Vaskovsky's method [18]. Gas–liquid chromatography (Mega 8180-O, Carlo Erba, Rodano, Italy) was used to differentiate between phospholipids with different fatty acyl chain compositions. Lipids were first hydrolysed in 5 N HCl, then, to increase their volatility, the resulting free fatty acids were converted to their respective methyl esters, using 10% acetylchloride in methanol [19]. Heptadecanoic acid (C_{17}), treated identically, was used as an internal standard.

3. Results

3.1. Crystal structure and size of the iron oxide cores

Both iron oxide preparations crystallized in the inverse spinel structure (space group $Fd\overline{3}m$), as shown by powder x-ray diffraction studies using Cu Kα_1 radiation at room temperature (figure 1). Although air oxidation was reported to cause considerable conversion of Fe_3O_4 to γ-Fe_2O_3 [20], comparison of the observed reflections with regard to 2θ values and intensity with the theoretical values for Fe_3O_4 and γ-Fe_2O_3 showed that γ-Fe_2O_3 did not form in both cases; a reflection (110) at $2\theta = 15.00°$, which is typical of the presence of γ-Fe_2O_3, was not observed.

The mean crystal size was determined from Scherrer's formula. To this end, the half-widths of the five strongest reflections in each diffraction pattern were calculated with the program Winplotr (Beta Version LLB/May 1999). From the calculated half-width of each reflection and the corresponding one of the standard sample, the reflection half-width caused by the crystal size (β) can be determined for each individual reflection, and used for correcting the reflection half-width for instrumental broadening [15]. The mean crystal sizes ($\overline{\varnothing}$) corresponding to each β value were then calculated. An overview of the data is presented in table 1.

Applying statistics to the $\overline{\varnothing}$ values based on the individual reflections results in an averaged mean crystal size of 130 ($\pm$50) nm for the crystallites formed using method B. The large standard deviation on the averaged mean crystal size is a result of the decrease in reflection half-width with increasing crystal size (compare the lower curve in figure 1 with the upper one).

Using the same procedure, it appears that the particles produced by method KR have a diameter of 12.8 ($\pm$0.4) nm.

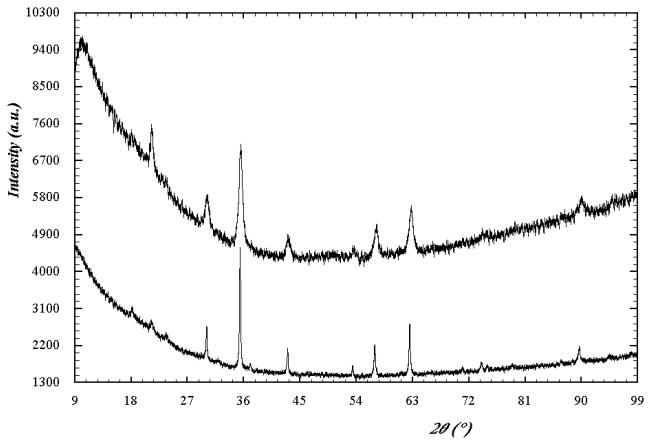

Figure 1. X-ray diffraction patterns of iron oxide cores prepared by method KR (above) and method B (below).

Table 1. Determination of the mean crystal size of the Fe_3O_4 cores prepared by the B and KR methods, using Scherrer's formula.

	Reflection half-width (deg)			$\beta(\times 100)$ (rad)		$\overline{\varnothing}$ (nm)	
2θ (deg)	Method KR	Method B	Standard sample	Method KR	Method B	Method KR	Method B
30.09	0.739	0.243	0.207	1.07	0.073	13.4	196.7
35.44	0.754	0.247	0.192	1.12	0.114	13.0	127.7
43.07	0.795	0.269	0.216	1.18	0.110	12.7	135.6
56.96	0.820	0.309	0.203	1.24	0.216	12.8	73.0
62.54	0.866	0.283	0.203	1.32	0.163	12.3	99.5

Transmission electron microscopy (Zeiss EM10C apparatus) was also used for size analysis of the Fe_3O_4 cores prepared by the KR method. To this end the diameter of about 2000 individual Fe_3O_4 crystals was measured. From the size distribution data (figure 2) an average diameter of 13.1 ($\pm$0.1) nm can be deduced. This value is in concert with the mean core size, calculated by Scherrer's formula (see above).

3.2. Magnetization and hysteresis of the iron oxide cores

The magnetization and hysteresis of the iron oxide cores prepared using methods B and KR were determined at room temperature in the applied field range of $\pm$2 T. In figure 3, only data points in the field range of $\pm$0.2 T are depicted.

The sample prepared using method B had a specific saturation magnetization σ = 94 A m^2 kg^{-1} at 2 T. This result agrees with earlier observations for Fe_3O_4 (92 A m^2 kg^{-1} at 2 T) [21, 22]. In addition, an hysteresis effect was observed with a remanence of 16 A m^2 kg^{-1}, reflecting a multi-domain structure of the particles. In contrast, the cores prepared using method KR showed no hysteresis, i.e. a behaviour typical of superparamagnetic subdomain Fe_3O_4. These results are in agreement with the diameters deduced from the x-ray studies (see above). Furthermore, the 19% lower saturation magnetization observed for the

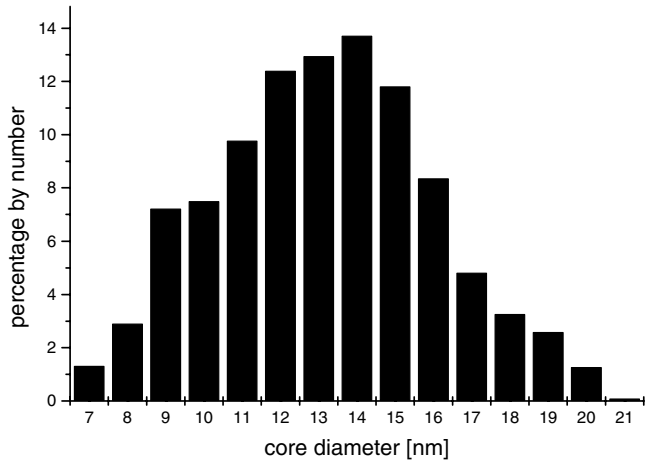

Figure 2. Size distribution by number of iron oxide cores prepared by method KR as deduced from the transmission electron micrographs. The diameter of 2200 particles was measured.

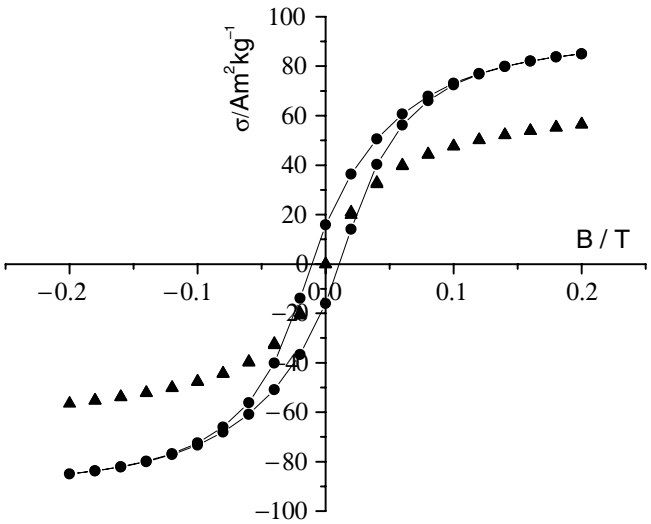

Figure 3. Specific magnetization as a function of the applied field at room temperature of iron oxide cores prepared by method KR (▲) and method B (●). Only data points in the field range from −0.2 to +0.2 T are depicted.

smaller particles ($\sigma = 76$ A m^2 kg^{-1}) can be explained by assuming that surface iron ions, which are supposed to be magnetically inactive, are relatively more abundant in smaller particles [23]. On the other hand, Coey and Khalafalla [24], who prepared and characterized fine superparamagnetic γ-Fe_2O_3 cores (mean diameter 6.5 nm), claimed that the low saturation magnetization originates from a significantly different spin arrangement in the fine particles as compared to that in bulk material, leading to a reduction of 15–17% in the magnetization.

3.3. Phospholipid transfer kinetics

The dynamics of the phospholipids in the coat were examined using magnetoliposomes with 13 nm Fe_3O_4 cores. Under the conditions used to construct the magnetoliposomes (47 mg of Fe_3O_4 and 228 mg of DMPC-DMPG (9/1)), a final phospholipid/Fe_3O_4 ratio of 0.80 mmol g^{-1} Fe_3O_4 was found after high-gradient magnetophoresis. For 13 nm cores, this corresponds to the formation of an intact phospholipid bilayer encircling the magnetite [2]. When these structures were mixed with an equimolar amount (with respect to phospholipid concentration) of pre-formed sonicated vesicles made from DMPC/DMPG/DPPE-PEG_{3400}-B (molar ratios 8:1:1), lipid transfer was observed. The kinetic profiles show that, at equilibrium, about 35% of the DPPE-PEG_{3400}-B was found in the acceptor magnetoliposome population (figure 4A). Treatment of the data points by first-order reaction formalism, which takes into account back transfer (see appendix), revealed $k_{+1} = 0.0032_2$ and 0.0037_7 min^{-1} for DPPE-PEG_{3400}-B magnetoliposome enrichment (figure 5, ●) and vesicle depletion (figure 5, ○), respectively, corresponding to $t_{1/2} = 107$ and 93 min.

In contrast, under identical conditions, no transfer of unmodified DPPE between vesicles and magnetoliposomes occurred within the timescale of the experiment (figure 4B).

4. Discussion

Magnetic nanometre-sized particles can be produced by a variety of techniques (see [25] and references cited therein). Recently, the production of uniform particles by precipitation in single-compartment vesicles, acting as nanoreactors, has been suggested to be a better method of preparing mono-dispersed grains [26]. In brief, in this technique, Fe^{2+} and Fe^{3+} salts are first captured in the inner space of the vesicles during sonication of phospholipids in an aqueous salt solution, the extra-vesicular reactant cations are removed by dialysis, gel permeation or ion-exchange column chromatography, and the pH of the medium is raised so that OH^- ions permeate the vesicle wall and react with the intra-vesicular cations to produce nano-sized precipitates until all cations are exhausted. We initially tried this method, but were unsuccessful, probably since some traps are inherently associated with the technique. For instance, in order to generate a sufficiently large iron particle that can be quantitatively attracted in a magnetic field, one has to start with highly concentrated solutions of ferrous and ferric salts. However, under these conditions, the pH is extremely low and this may hamper the integrity of both the vesicle structure and the phospholipid building blocks themselves (see, for instance, [19]). In addition, unsaturated phospholipids are reported to be highly susceptible to peroxidation induced by Fe ions [27, 28]. Furthermore, the association of Fe^{3+} and, to a somewhat lesser extent, Fe^{2+} ions with the phosphate group in phospholipid molecules is extremely high [2, 29], with the result that it is extremely difficult to completely remove these extra-vesicular ions, e.g. by dialysis or ion exchange chromatography. On increasing the pH, these residual ions precipitate, together with the phospholipid structures, thereby forming irreversible phospholipid–magnetite clusters.

In contrast, the two different co-precipitation protocols used in this work, in our hands, proved highly reliable and produced magnetite particles of different (13 and 130 nm), but uniform, sizes. The theoretical Fe^{2+}/Fe^{3+} ratio in magnetite is 0.5. Although we started with a ratio of 0.67, we ended up with Fe_3O_4, as shown by the x-ray diffraction pattern. As mentioned by Khalafalla and Reimers [9], it is likely that Fe^{2+} becomes partially oxidized during the preparation of the magnetic fluid in air.

The bigger size of the 130 nm particles and the presence of remanent magnetism after their exposure to a magnetic field (figure 2) seriously hinders their colloidal dispersibility, and,

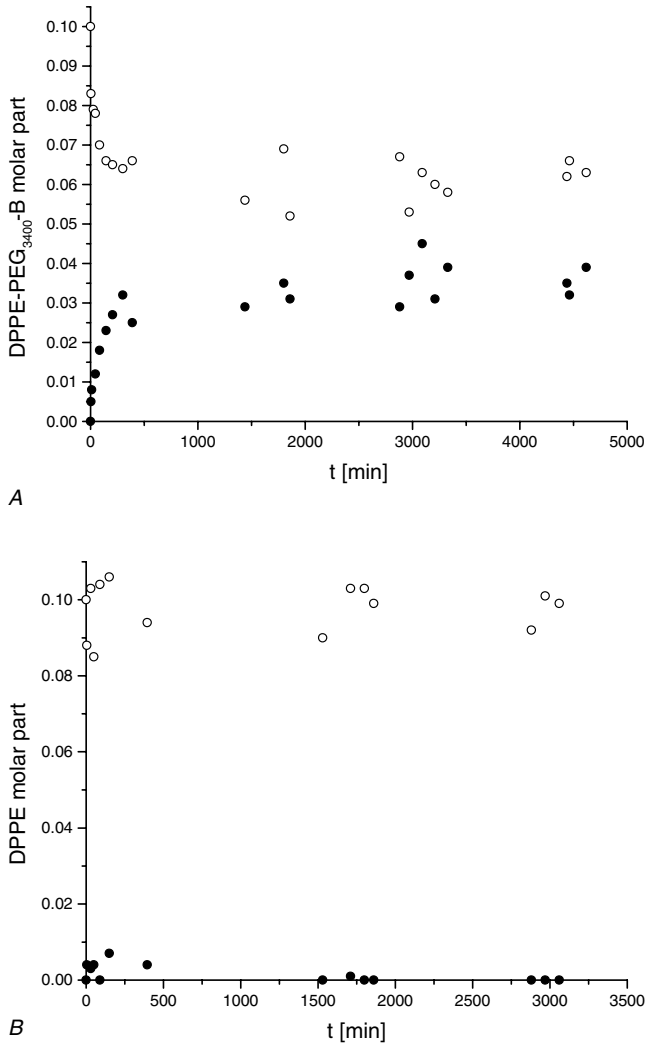

Figure 4. Transfer of DPPE-PEG_{3400}-B (A) or DPPE (B) from DMPC/DMPG/DPPE-PEG_{3400}-B (molar ratio 8/1/1) or DMPC/DMPG/DPPE (8/1/1) donor vesicles, respectively, to DMPC/DMPG (9/1) magnetoliposomes. The circles represent the time-dependent changes in the fractional amount of DPPE-PEG_{3400}-B (A) or DPPE (B) in the vesicles (○) and the magnetoliposomes (●). The experiments were performed at 25 °C in 5 mM TES buffer, pH 7.0. In the kinetic incubation mixture, donors and acceptors were present at equimolar amounts with respect to phospholipid content.

consequently, may restrict their medical applicability [30]. In addition, since in hyperthermia experiments heat generation is inversely related to particle size, we decided to use the smaller iron oxide cores, prepared according to the KR method, to produce magnetoliposomes.

Following our protocol for the preparation of magnetoliposomes, we found that all the magnetic spheres were covered by a phospholipid bilayer. This means that the encapsulation can be considered to be 100%. This high value contrasts significantly with the much lower values generally obtained if magnetic cores are encaged in phospholipid vesicles during the generation of the latter. For instance, Domingo *et al* [31], who claimed superior efficiency, achieved a value for encapsulation of only 16%.

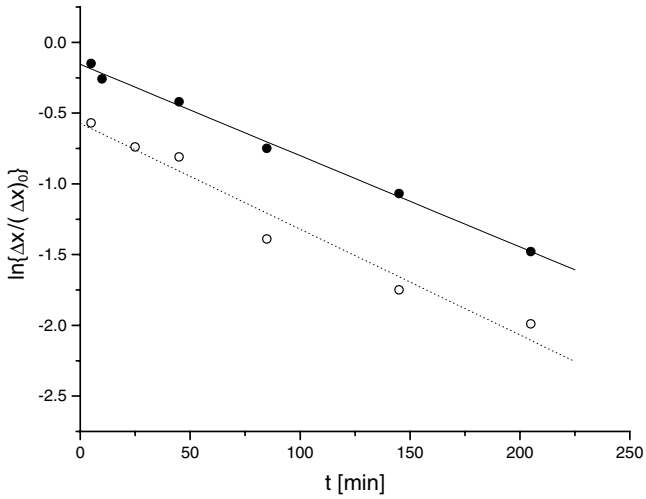

Figure 5. First-order kinetic plot of DPPE-PEG_{3400}-B depletion from donor vesicles (○) and DPPE-PEG_{3400}-B enrichment of the magnetoliposome acceptors (●), as illustrated in figure 4A. The straight line was drawn by a least squares fit. The meaning of the *y* axis is explained in the appendix.

Therapeutic *in vivo* application of magnetic nanospheres in cancer therapy, blood purification, lymph node imaging or hyperthermia, to name just a few, requires the particles to be biocompatible and non-toxic. Magnetoliposomes are excellent candidates for these purposes. Iron oxide seems to be well tolerated [32–34] and the coating consists of phospholipids that adopt an identical architecture to that found in natural membranes, i.e. a bilayer configuration.

The present results also show that an additional and most interesting feature of these structures is that, once prepared from common phospholipids, the mantle on the particle surface can be further fine-tuned in a very simple way without the need for chemical manipulations. Flexibility in surface characteristics may be of prime importance, for instance, if, for targeting and/or imaging purposes, the biocolloids have to circulate in the body for a long time. As mentioned in the introduction, (magneto)liposome uptake by the liver can be dramatically retarded by the incorporation of a small percentage of PEGylated phospholipids. The present work shows that such magnetoliposome coat modification can be readily performed by mixing magnetoliposomes with pre-formed vesicles containing relevant PEGylated molecules. To study this inter-membrane phospholipid transfer, we carefully chose donors and acceptors made of host phospholipids that were above their gel-to-liquid crystalline phase transition temperature (T_t), which is 23 °C for both DMPC and DMPG [35]. In this way, interference due to aggregate formation between 'solid' membrane structures below their T_t could be avoided. At equilibrium, DPPE-PEG_{3400}-B was distributed in a 2/1 ratio between vesicle donors and magnetoliposome acceptors, suggesting that only the lipids residing in the outer vesicle layer participated in the overall percolation phenomenon and, thus, that trans-bilayer flip–flop movement did not occur within the timescale of the experiment. This behaviour can be explained by assuming that the thermodynamic energy barrier for the polar head-group of the inner leaflet phospholipids to cross the hydrophobic region of the membrane is too high to be overcome [36].

The fact that the kinetics obeyed exponential first-order reaction rules also points to lipid movement through the aqueous phase in the form of free monomers and excludes a collision-

mediated process [37, 38]. The proposed so-called aqueous transfer mechanism assumes that the phospholipid escapes into the aqueous medium, then passes, by diffusion-controlled transfer, to the acceptor membrane, where it is resorbed. Within the overall event, the rate-limiting step is the desorption step. In agreement with this picture, we found that the transfer rate clearly depended on the polar/apolar nature of the moving lipid, since PEGylation of DPPE, which increases its water solubility, dramatically improved its ability to leave the donor membrane. Alternatively, though not investigated in this work, the length of the apolar phospholipid tails, too, is of paramount importance. In general, removal of one $–CH_2–$ from the acyl chain results in a 6.3-fold improvement in transfer [39]. Furthermore, under similar experimental conditions, we have previously found that the transfer halftimes of DMPC and DMPG, which—in the present work—act in the SUVs and magnetoliposomes as matrix phospholipids of both donors and acceptor membranes, are 90 and 41 min [40]. In the present set-up, inter-membrane percolation of host phospholipids was not monitored, but, in light of the above-mentioned low $t_{1/2}$ values, we assume a fast, symmetrical inter-membrane lipid movement for both lipid types. An important consequence of this highly dynamic behaviour is the likelihood that the properties of donors and acceptor bilayers do not change significantly during transfer, and, therefore, there is no change in the magnitude of the rate constants during transfer. Thus, the data points used in the kinetic calculations are not restricted to the initial phase of transfer, as is often the case (e.g. [40]), but can cover the whole process until lipid mixing approaches equilibrium (see the appendix).

Acknowledgments

We would like to thank Mr Karol Korczak and Mr Lech Swinder for assistance with the magnetization and diffractometry measurements, respectively. The financial support of the Flemish *Fonds voor Wetenschappelijk Onderzoek* (grant no G.0170.96) and Fonds der Chemischen Industrie is gratefully acknowledged.

Appendix. Reversible first-order phospholipid exchange

The reversible exchange of a particular phospholipid species (PL) between donors (D) and acceptors (A) can be simply represented by the following reaction equation.

$$\mathrm{PL}_D \rightleftharpoons \mathrm{PL}_A. \tag{A.1}$$

In those cases in which the phospholipid partition is not drastically shifted towards the acceptor population at equilibrium, the 'backward' reaction has to be taken into account in the kinetic treatment of the reaction. The rate constants for the 'forward' and 'backward' reactions are k_{+1} and k_{-1}, respectively.

In the following derivation, it is assumed that, at $t = 0$, no PEGylated lipid is present in the acceptors. The concentrations of PEGylated lipid in the donors (c_D) and acceptors (c_A) at $t = 0$, at any time, t, during the transfer event, and at equilibrium ($t \to \infty$) are given in the following scheme. More precisely, the concentration of PEGylated phospholipid refers to the fraction of the PEGylated lipid in the *outer* shell of the phospholipid bilayer, since, within the time period covered, the phospholipids in the inner leaflet do not participate in the inter-membrane exchange process (see the discussion).

The relationship between the different concentrations is as follows:

$$(c_D)_0 = c_D + c_A = (c_D)_\infty + (c_A)_\infty. \tag{A.2}$$

Table A.1. Symbols, representing the fraction of PEGylated lipid in the outer shell of the magnetoliposome acceptors (A) and vesicle donors (D) at time = 0, any time t and at equilibrium (∞).

T	c_D	c_A
0	$(c_D)_0$	$(c_A)_0$
t	c_D	c_A
∞	$(c_D)_\infty$	$(c_A)_\infty$

At each time-point during the process, the overall rate, r, is determined by the difference between phospholipid removal from the donors and phospholipid incorporation into the acceptors per time unit.

$$r = -\frac{\mathrm{d}c_D}{\mathrm{d}t} = k_{+1}c_D - k_{-1}c_A. \tag{A.3}$$

At equilibrium, $r = 0$ so

$$k_{+1}(c_D)_\infty = k_{-1}(c_A)_\infty \tag{A.4}$$

and

$$K = \frac{k_{+1}}{k_{-1}} = \frac{(c_A)_\infty}{(c_D)_\infty}. \tag{A.5}$$

Expression of c_A as a function of c_D and of the equilibrium concentrations (equation (A.2)) and substitution in (A.3) yields

$$\frac{-\mathrm{d}c_D}{\mathrm{d}t} = k_{+1}c_D - k_{-1}[(c_D)_\infty + (c_A)_\infty - c_D] = (k_+ + k_{-1})c_D - k_{-1}(c_D)_\infty - k_{-1}(c_A)_\infty. \tag{A.6}$$

In the special case of lipid transfer between two vesicle populations with the same curvature and lipid composition, it is reasonable to assume that k_{+1} is equal to k_{-1} and that $(c_D)_\infty$ is equal to $(c_A)_\infty$. Equation (A.6) can then be simplified to

$$\frac{-\mathrm{d}c_D}{\mathrm{d}t} = 2k_{+1}[c_D - (c_D)_\infty]. \tag{A.7}$$

Integration of (A.7) gives

$$\int \frac{\mathrm{d}c_D}{c_D - (c_D)_\infty} = -2k_{+1}\int \mathrm{d}t. \tag{A.8}$$

Taking into account the conditions at $t = 0$, this gives

$$\ln[c_D - (c_D)_\infty] = \ln[(c_D)_0 - (c_D)_\infty] - 2k_{+1}t. \tag{A.9}$$

If Δx is defined as the deviation from equilibrium

$$\Delta x = c_D - (c_D)_\infty = (c_A)_\infty - c_A \tag{A.10}$$

then (A.9) can be expressed as

$$\ln(\Delta x) = \ln(\Delta x)_0 - 2k_{+1}t \tag{A.11}$$

or

$$\Delta x = (\Delta x)_0 \mathrm{e}^{-2k_{+1}t}. \tag{A.12}$$

From the latter equations, it follows that Δx decays according to first-order kinetics rules.

References

[1] Bangham A D, Standish M M and Watkins J C 1965 *J. Mol. Biol.* **13** 238–52
[2] De Cuyper M and Joniau M 1988 *Eur. J. Biophys.* **15** 311–19
[3] Kulkarni S B, Betageri G V and Singh M 1995 *J. Microencapsul.* **12** 229–46
[4] De Cuyper M, De Meulenaer B, Van der Meeren P and Vanderdeelen J 1996 *Biotechnol. Bioeng.* **49** 654–8
[5] Bulte J W M, De Cuyper M, Despres D, Brooks R A and Frank J A 1999 *J. Magn. Reson. Imaging* **9** 329–35
[6] Müller-Schulte D, Füssl F, Lueken H and De Cuyper M 1997 *Scientific and Clinical Applications of Magnetic Carriers* ed U Häfeli, W Schütt, J Teller and M Zborowski (New York: Plenum) pp 517–26
[7] Allen T M 1996 *Curr. Opin. Colloid Interface Sci.* **1** 645–51
[8] Hodenius M, De Cuyper M, Desender L, Müller-Schulte D, Steigel A and Lueken H 2002 *Chem. Phys. Lipids* **120** 75–85
[9] Khalafalla S E and Reimers G W 1980 *IEEE Trans. Magn.* **16** 178–83
[10] Bergemann C 1996 *German Patent* DE 19624426 A1 8
[11] Yvon K, Jeitschko W and Parthé E 1977 *J. Appl. Crystallogr.* **10** 73–4
[12] Fleet M E 1981 *Acta Crystallogr.* B **37** 917–20
[13] Shin H-S 1998 *J. Kor. Ceram. Soc.* **35** 1113–19
[14] Scherrer P 1918 *Nachr. ges. Wiss. Göttingen, Math.-Phys. Kl.* **2** 98–100
[15] Lipson H and Steeple H 1970 *Interpretation of X-Ray-Powder Diffraction Patterns* (London: MacMillan) p 258
[16] Nelson D and ter Haar L W 1993 *Inorg. Chem.* **32** 182–8
[17] Yoe J H and Jones A L 1944 *Ind. Eng. Chem. Anal. Ed.* **16** 111–15
[18] Vaskovsky V E, Kostetsky E Y and Vasendin I M 1975 *J. Chromatogr.* **114** 129–41
[19] Christie W W 1982 *Lipid Analysis: Isolation, Separation, Identification and Structural Analysis of Lipids* 2nd edn (Oxford: Pergamon)
[20] Massart R and Cabuil V 1987 *J. Chim. Phys.* **84** 967–73
[21] Smit J and Wijn H P J 1959 *Ferrites* (London: Cleaver-Hume) p 157
[22] Pauthenet R 1950 *C. R. Acad. Sci., Paris* **230** 1842–3
[23] Sato T, Iljima T, Seki M and Inagaki N 1987 *J. Magn. Magn. Mater.* **65** 252–6
[24] Coey J M D and Khalafalla D 1972 *Phys. Status Solidi* **11** 229–41
[25] Yaacob I I, Nunes A C, Bose A and Shah D O 1994 *J. Colloid Interface Sci.* **168** 289–301
[26] Sangregorio C, Wiemann J K, O'Connor C J and Rosenzweig Z 1999 *J. Appl. Phys.* **85** 5699–701
[27] Vasiljeva O V 2000 *Membr. Cell Biol.* **14** 47–56
[28] Li Q T 2000 *Biochem. Biophys. Res. Commun.* **273** 72–6
[29] Tadolini B, Motta P and Rossi C A 1993 *Biochem. Mol. Biol. Int.* **29** 299–305
[30] Häfeli U and Pauer G J 1999 *J. Magn. Magn. Mater.* **194** 76–82
[31] Domingo J C, Mercadal M, Petriz J and De Madriaga 2001 *J. Microencapsul.* **18** 41–54
[32] Weissleider R, Stark D D, Engelstad B L, Bacon B R, Compton C C and White D L 1989 *Am. J. Roentgenol.* **152** 167–73
[33] Garcia V A P, Lacava L M, Kückelhaus S, Azevedo R B, Da Silva M F, Morais P C, De Cuyper M and Lacava Z G M 2002 *Eur. Cells Mater.* **3** 154–5
[34] Wagner S, Schnor J, Pilgrimm H, Hamm B and Taupitz M 2002 *Invest. Radiol.* **37** 167–77
[35] Boggs J M 1980 *Can. J. Biochem.* **58** 755–70
[36] Wimley W C and Thompson T E 1990 *Biochemistry* **29** 1296–303
[37] Nichols J W and Pagano R E 1981 *Biochemistry* **20** 2783–9
[38] De Cuyper M, Joniau M and Dangreau H 1983 *Biochemistry* **22** 415–20
[39] Silvius J R and Zuckermann M J 1993 *Biochemistry* **32** 3153–61
[40] De Cuyper M, Joniau M, Engberts J B F N and Sudhölter E J R 1984 *Colloids Surf.* **10** 313–19